Nanoscale Topographic Instabilities of a Phospholipid Monolayer

W. R. Schief,[†] L. Touryan,[‡] S. B. Hall,[§] and V. Vogel*[,†,‡]

Departments of Physics and Bioengineering, University of Washington, Seattle, Washington 98195, and Departments of Biochemistry and Molecular Biology, Medicine, and Physiology and Pharmacology, Oregon Health Sciences University, Portland, Oregon 97201

Received: October 22, 1999

Light scattering microscopy reveals previously undetected topographic instabilities in phospholipid monolayers at the air/water interface far below the collapse pressure. Following compression through the fluid → condensed phase transition in monolayers of dipalmitoyl phosphatidylcholine, after the disappearance of the fluid phase, the contact regions between condensed domains acquire static roughness as indicated by enhanced light scattering. With further compression, a nanoscale budding process occurs within the roughened regions, while the interiors of the condensed domains remain flat and retain their domain shapes. At monolayer collapse, the buds proliferate across the entire interface, suggesting that the buds detected at lower pressures represent spatially confined fluctuations into the collapse phase. The confinement of static roughness formation and budding to domain contact regions indicates that these topographic instabilities originate from packing defects created where adjacent domain edges with conflicting molecular orientations grow together during the fluid → condensed phase transition.

Introduction

Lipid monolayers at the air/water interface are important systems for the study of ordering and phase transitions in two dimensions.[1,2] They also display a variety of "collapse" transitions into three dimensions.[3] Below the collapse pressure, the only known topographic transition is monolayer buckling which seems to require unusually high compressional rigidity.[4,5] Otherwise, condensed lipid monolayers at the air/water interface are not known to possess topographic features beyond the plane aside from thermal fluctuations. When isothermally compressed above their triple point, lipid monolayers pass through a first-order phase transition, from liquid-expanded (LE) → tilted-condensed (TC).[1,2] The molecular orientations at the edges of adjacent TC domains are not aligned in general, so after the disappearance of the LE phase a condensed film may contain packing defects in the contact regions where TC domains grew together. We therefore hypothesized that condensed lipid monolayers in the TC phase might yield into the third dimension at the boundaries between formerly distinct TC domains, at pressures below collapse. To test this hypothesis, we implemented a highly sensitive version of dark field microscopy[6] that we call light scattering microscopy (LSM). LSM forms an image of the monolayer by illuminating the interface with a laser at an oblique angle and collecting scattered light distributed about the surface normal (Figure 1). When the low background scattering at the air/water interface is taken advantage of and an intensified CCD camera is combined with a relatively powerful laser (90 mW incident on water), LSM can detect topographic variations on the angstrom scale.[7]

With a combination of LSM, Brewster angle microscopy (BAM),[8,9] and atomic force microscopy (AFM) we have examined monolayers of the widely studied phospholipid dipalmitoyl phosphatidylcholine (L-DPPC). In these films, TC domains in coexistence with the LE phase have chiral shapes[10,11] in which the in-plane tilt orientation exhibits a splay across the curved domain arms,[12,13] so adjacent domain edges have conflicting molecular orientations. Furthermore, in condensed L-DPPC monolayers a chain tilt from the surface normal persists to the collapse pressure.[14] During compression in the TC phase of L-DPPC (after the disappearance of the LE phase) LSM reveals two nanoscale topographic instabilities that are spatially localized in the regions of contact between formerly distinct TC domains. Far below the monolayer collapse pressure, regions surrounding chiral-shaped domains first acquire static roughness and then undergo nanoscale budding upon monolayer compres-

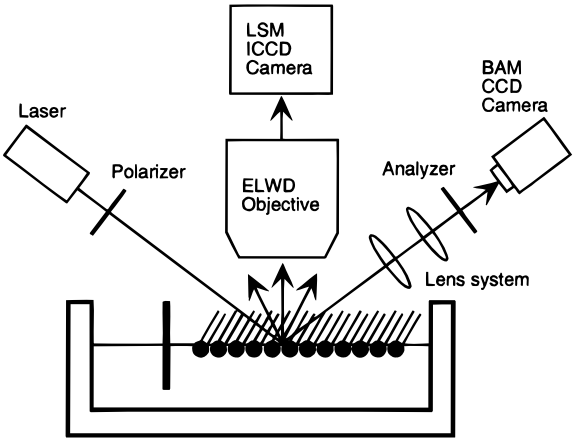

Figure 1. Schematic of Brewster angle microscopy (BAM) and light-scattering microscopy (LSM). BAM allows visualization of microscopic structure and chain-tilt ordering in molecular monolayers by imaging the reflectivity to p-polarized light with nearly zero background at Brewster's angle. LSM allows visualization of topographic features on the nanoscale level that are invisible in BAM by imaging the monolayer via the scattering about the surface normal.

* Corresponding author: Department of Bioengineering, University of Washington, Box 352125, Seattle, WA 98195. Phone: (206) 543-1776. Fax: (206) 685-4434. E-mail: vvogel@u.washington.edu.
[†] Department of Physics, University of Washington.
[‡] Department of Bioengineering, University of Washington.
[§] Oregon Health Sciences University.

10.1021/jp993770+ CCC: $19.00
Published on Web 07/19/2000

sion. The chiral domains, which possess shapes characteristic for the TC domains of L-DPPC, maintain their shapes and avoid static roughness formation and budding until monolayer collapse. Control experiments demonstrate that these results are not due to sample or experimental artifact. These findings illustrate previously undetected topographic complexity in phospholipid monolayers and are consistent with the hypothesis that topographic instabilities may originate from packing defects created at the boundary of TC domains during the LE → TC transition.

Our observations are also significant because L-DPPC monolayers are widely used models for the pulmonary surfactant film that maintains high surface pressures in the lung,[15,16] and L-DPPC bilayers are prevalent in the study of lipid membranes.[17] The nanoscale topographic instabilities occur over a wide surface pressure range spanning the pressures considered relevant to these systems.

Materials and Methods

Langmuir Trough and Solutions. Monolayers of L-DPPC (>99%, Avanti Polar Lipids, Sigma) were spread on water (resistivity >18.0 MΩ, pH 5.6) and on buffer (10 mM Hepes, 150 mM NaCl, 1.5 mM $CaCl_2$, pH 7.0) in a custom-built Teflon trough (maximum area = 532 cm^2) with a continuous perimeter, vertical Teflon ribbon (Labcon, Darlington, UK) to contain the film. All experiments were performed at room temperature (20−22 °C). Continuous compression or expansion at a rate of 0.6 $Å^2$/molecule/min was employed except where noted otherwise. To lessen the surface flow anisotropy due to uniaxial compression from one end of the trough, we have placed two small (0.5 × 2 cm) Teflon blocks in the observation area of the trough. This allowed the shapes of the domains visualized with LSM in L-DPPC above $\pi = 13$ mN/m (Figure 2) to remain essentially undistorted up to the collapse pressure. The topographic instabilities in L-DPPC were found to occur similarly in the presence or absence of these blocks. Experiments with control monolayers were performed with the blocks. Control monolayers (>99%) of dimyristyl phosphatidylethanolamine (L-DMPE, Avanti) and pentadecanoic acid (PDA, Sigma) on water as well as dipalmitoyl phosphatidylglycerol (L-DPPG, Avanti) on buffer (10 mM Hepes, 150 mM NaCl, pH 7.4, both with and without 1.5 mM $CaCl_2$) were examined with BAM-LSM under experimental conditions similar to those for L-DPPC. Buffer and all salts were purchased from Sigma (SigmaUltra). The trough and microscopes described below rested on active electronic vibration isolation tables (Nanofilm Technologie, MOD 2).

Brewster Angle Microscopy (BAM). A home-built Brewster angle microscope was mounted on the Langmuir trough (see Figure 1). A laser beam of wavelength 532 nm (Coherent DPSS 532-100) set to p-polarization with a Glan-Thompson polarizer provided a power of ~90 mW incident on the air−buffer interface at Brewster's angle ($\theta = \tan^{-1}(n_{buffer}/n_{air}) \approx 53.1°$ from the surface normal). Obtaining a coincident focus of the BAM and LSM required a long working distance in both microscopes. For BAM, the reflected light was focused by a system of two single lenses (Spindler & Hoyer) with a working distance of ~65 mm through a Glan-Thompson analyzer onto a CCD camera (Dage-MTI, CCD-72). The BAM CCD camera was tilted in the plane of incidence to correct for the magnification asymmetry induced by imaging at an angle.

Light Scattering Microscopy (LSM). LSM examined the same surface location as the BAM. Light from the BAM laser scattered about the surface normal was focused by an objective (Nikon, NA = 0.45, working distance = 9 mm) onto an image intensifier (Intevac Nitemate 1306) coupled to a CCD camera (Pulnix TM-745G). Minimization of the background scattered light was critical in order to observe the topographic transitions. The transmitted laser beam was reflected away from the LSM objective and out of the subphase with two mirrors (Spindler & Hoyer) mounted on the trough bottom.

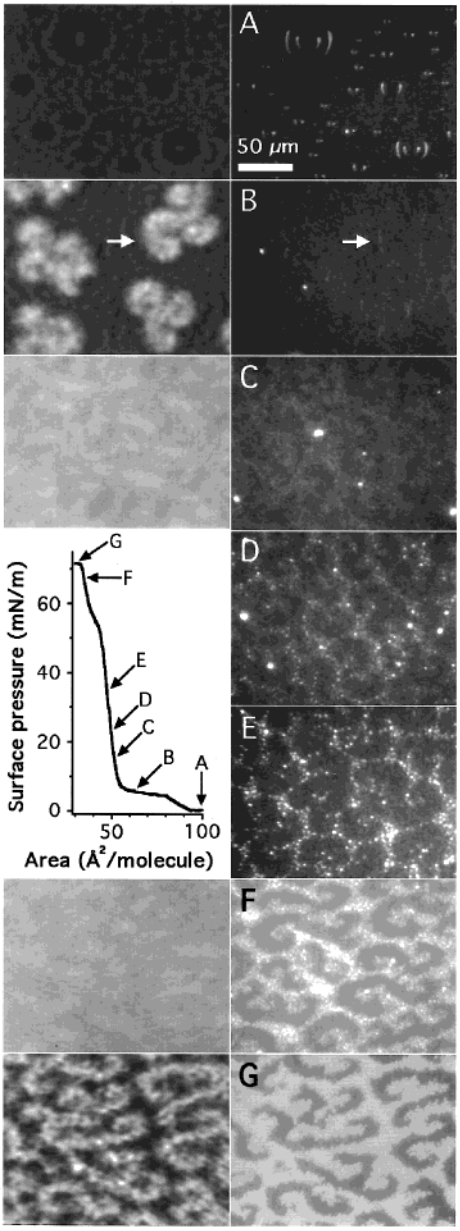

Figure 2. Visualization of topographic changes in L-DPPC monolayers compressed on a buffer. BAM−LSM image pairs are shown from the same surface location at increasing surface pressure. BAM images with an analyzer at "p" on the left, corresponding LSM images on right. The white scale bar (50 μm) applies to all images. Displayed images were recorded at the following surface pressures (mN/m): A, 0.2; B, 5.5; C, 15.6; D, 22.7; E, 34.9; F, 67.3; G, 71.0. The π−A isotherm of L-DPPC on buffer at 22 °C is shown in the middle left. White arrows in B indicate one TC domain edge visible in LSM. The BAM images corresponding to LSM images D and E show essentially uniform grayscale similar to that of the BAM images C and F. The few very bright individual scattering centers apparent in LSM images B and C are nonlipid particles that also are found in control experiments with no monolayer.[36] Relative intensities have been preserved in LSM images A-E, but F and G were recorded with a reduced camera gain.

Atomic Force Microscopy (AFM). L-DPPC monolayers transferred onto freshly cleaved mica by the Langmuir−Blodgett technique on the upstroke at 14 mm/min were examined in air with tapping mode AFM (Digital Instruments, Santa Barbara,

CA). For transfer experiments, Nanopure water (resistivity >18.0 MΩ, pH 5.6) was used as a subphase instead of buffer in order to avoid salt crystallization under the transferred film.[18] In most cases, the monolayer at the air/water interface was observed with LSM−BAM imaging before, during, and after transfer. Transferred layers were stored under ambient conditions and examined from 12 h to several days after transfer, with no detectable differences due to aging in films transferred at π = 15 mN/m and above.

Results and Discussion

Gas → LE and LE → TC Transitions. LSM and BAM simultaneously imaged L-DPPC monolayers on both water and buffer. BAM−LSM image pairs show the familiar gas/LE coexistence (Figure 2A) and LE/TC coexistence (Figure 2B). At $\pi \leq 0.3$ mN/m, the two-dimensional gas phase surrounded by the optically thicker LE phase appears dark on a lighter background in BAM. The edges of the gas bubbles appear as bright "parentheses" in LSM because the plane of laser incidence is horizontal.[19] TC domains surrounded by the LE phase at $\pi = 5.5$ mN/m within the isotherm plateau show typical, chiral L-DPPC domain shapes[10,11,13] in BAM. Edges of the TC domains which are nearly perpendicular to the laser direction are faintly visible in LSM.[20] The lower LSM contrast for the LE/TC edge as compared to the gas/LE edge (∼50% less intensity above background) is due to smaller differences in height and density across the LE/TC edge. Within the TC domains, the in-plane tilt orientation has a curvature that parallels the spiral domain arms and exhibits a splay across the width of each arm.[12,13] The chain tilt from the surface normal is 30° at $\pi = 40$ mN/m[21] in the pure TC phase, and although the tilt of phospholipid TC phases generally declines with compression,[1] the L-DPPC chains do not reach an untilted state, even at $\pi = 71$ mN/m.[14]

Emergence of Spatially Confined Static Roughness. After completion of the LE → TC transition and the corresponding loss of edge contrast in LSM at $\pi = 11 \pm 1$ mN/m (not shown), LSM reveals the formation of spatially confined static roughness at $\pi = 13$ mN/m. Diffuse scattering from about half the monolayer (Figure 2C, right column) suddenly increases. The continuous region of increased scattering surrounds darker, chiral domains that possess the same range of morphologies as the domains typically found in the LE/TC coexistence region (previously noted in Figure 2B). The scattering from both the domains and the brighter surrounding region appears spatially uniform with the current LSM lateral resolution of 2.5 μm. The dark domains are visible up to the collapse pressure $\pi \geq 71$ mN/m, and the spatially uniform increased scattering surrounding the domains is visible until π = 60 mN/m when it is obscured by the proliferation of buds (see "**Budding Transition**"). In a separate publication, the intensities in LSM images were quantitatively analyzed to determine the topographic structure of the domains and the brighter surrounding.[7] We showed there that the domains possess only thermal roughness within the range of surface wavelengths that diffract into the LSM objective ($0.43 \leq \lambda \leq 1.52$ μm), and therefore the domains are flat in a time-averaged sense. We further demonstrated that the increased scattering from the surrounding region corresponds to a small, permanent roughness that is superimposed on the thermal roughness. If the static roughness is described by a Fourier expansion of surface modes, we showed[7] that the scattered intensity indicates a rms roughness amplitude less than 0.5 Å within the surface wavelengths that diffract into the LSM. Here, we show that the static roughness does not give rise to contrast in BAM. The BAM image of Figure 2C is essentially uniform. The slight variations in BAM grayscale are due largely to the differences in p-polarized reflectivity of tilted lipid chains with different in-plane orientations. Reflection microscopy does not detect a decrease in reflectivity and low angle scattering from the roughened region, as expected for such a weak surface deformation.

Budding Transition. A third topographic feature, in addition to the flat domains and the roughened surrounding, appears with compression above $\pi = 20 \pm 1$ mN/m. Bright point scatterers emerge in LSM within the roughened region (Figure 2D), increase in number from $\pi = 20$ to $\pi = 32$ mN/m (Figure 2E), and then remain constant in number until $\pi = 60$ mN/m (Figure 3A). Above a threshold of $\pi = 60$ mN/m, the point scatterers proliferate in the roughened region (Figure 2F,G), and their number increases steeply with surface pressure (Figure 3A). Their bright intensity in LSM indicates that the point scatterers are three-dimensional. Tapping-mode AFM analysis of films transferred to mica (Figure 4) shows that the individual scatterers correspond to one or several multi-bilayer islands with diameters in the range 15−150 nm. Considering the sensitivity of the LSM to approximately angstrom level roughness,[7] it is not surprising that such small particles are detectable. The LSM intensity distribution of the point scatterers (Figure 3C) remains unchanged during compression from $\pi = 20$ mN/m at which the point scatterers first emerge to $\pi = 60$ mN/m. This observation indicates that the scatterers do not continue to grow following nucleation, even while their number detected by LSM remains essentially constant between $\pi = 32$ and $\pi = 60$ mN/m. Consistent with submicron sizes, BAM does not resolve the individual point scatterers. The BAM images remain homogeneous (Figure 2F, $\pi = 67.3$ mN/m) until the density of the point scatterers rises sufficiently that their scattering measurably reduces the light intensity reflected and scattered into the BAM aperture (Figure 2G, $\pi = 71.0$ mN/m).

Consistent with previously measured isotherms of L-DPPC,[10,12] we find no detectable change of slope (Figure 2) corresponding to the emergence of point scatterers at $\pi = 20$ mN/m or to the halt in production at $\pi = 32$ mN/m. The material entering the point scatterers between $\pi = 20$ and $\pi = 32$ mN/m therefore must amount to less than ∼1% of the monolayer area. The isotherm shoulder at $\pi \sim 55$ mN/m indicates leakage onto the barrier of the ribbon trough rather than a phase transition.[22,23]

Two observations indicate that these point scatterers form via a budding[24,25] process involving the bending of the monolayer into protrusions the majority of which are connected to the monolayer by a neck. First, the proliferation of scatterers above $\pi = 60$ mN/m is reversible (Figure 3A). If the scatterers represented nanocrystals or another three-dimensional structure formed by reassembly of expelled lipids, they could not readily reincorporate into the monolayer upon expansion in the pressure range $60 \leq \pi \leq 71$, due to insufficient surface tension ($\gamma = 72 - \pi$) to draw material into the film. Indeed, the equilibrium spreading pressure of L-DPPC is $\pi_e \sim 0$ mN/m below the gel−liquid crystal transition temperature $T_c = 41$ °C and $\pi_e \sim 48$ mN/m above T_c.[26] In contrast, buds that remain connected to the monolayer by a neck and possess high bending energy will exert a "reinsertion pressure" on the monolayer, driving their reincorporation upon expansion. The low spontaneous curvature of the molecule, evidenced by the fact that no hexagonal or cubic phases have been found for dispersions of L-DPPC in water,[17] indicates that nanoscale buds of L-DPPC would possess high bending energy. Second, the halt in production of point

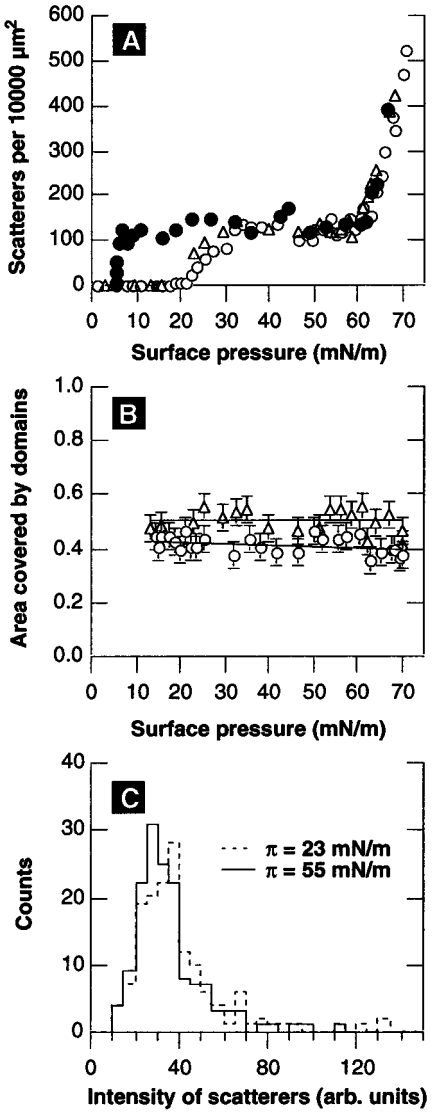

Figure 3. Surface pressure-induced changes in the topographic structure of L-DPPC monolayers. (A) Number of point scatterers per 10 000 μm^2 in LSM images versus surface pressure for different experiments compressed to $\pi = 71$ mN/m. Open circles and triangles denote compression to $\pi = 71$ mN/m for two different experiments; closed circles show expansion for one experiment. Point scatterers were counted manually within a circle of diameter 210 μm using NIH Image.[37] Estimated errors are similar to the symbol size. The increase in scatterers upon collapse at $\pi \geq 71$ mN/m is not shown. Nonlipid particles accounted for 1−3 scatterers per 10 000 μm^2. (B) Fractional area covered by the dark domains versus surface pressure during compression for two different experiments (circles and triangles). Areas were measured in NIH Image.[37] The best linear fits were $A_{domains}$ (circles) = 0.44 (±0.02) − π*0.0006 (±0.0005) and $A_{domains}$ (triangles) = 0.51 (±0.03) − π*0.0001 (±0.0006). (C) Intensity distribution for point scatterers in LSM images at $\pi = 23$ and 55 mN/m. Intensities were measured for individual scatterers from image intensity profiles of single-pixel width and are given as the peak above the background. The total number of counts in each histogram is 150.

scatterers at $\pi = 32$ mN/m coincides with the emergence of a monolayer bending rigidity indicated by an X-ray reflectivity study of L-DPPC monolayers in the same range of π.[27] Since budding requires monolayer bending, the emergence of a bending rigidity should inhibit or prevent the budding process. As evidence that the buds form upward, away from the water, downward focusing of the LSM objective by ~100 μm failed to detect excess scattering particles above the low background in the subphase prior to collapse at $\pi \geq 71$ mN/m.

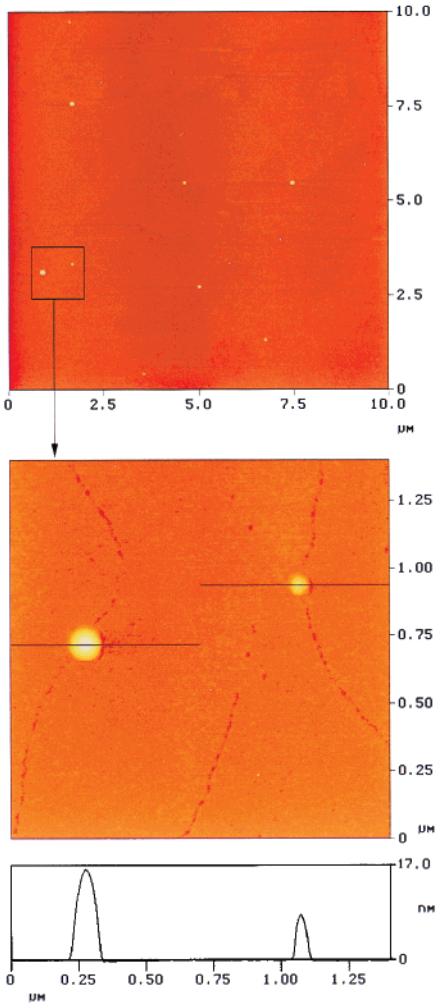

Figure 4. Nanoscale multibilayer islands detected by tapping-mode AFM on L-DPPC monolayers transferred to mica. Films transferred from a Nanopure water subphase onto freshly cleaved mica by the Langmuir−Blodgett technique on the upstroke at 14 mm/min were examined in air with tapping-mode AFM. Transfers were made at π = 5, 15, 30, 40, and 65 mN/m. On samples transferred at $\pi = 30$ mN/m and above, AFM detected nearly round islands with base diameters mostly in the range 15−150 nm. Islands with diameter ≥~50 nm showed heights ranging from 5 to 20 nm that were generally distributed in multiples of 4−6 nm, indicating bilayer and multibilayer structures. Islands with diameter <~50 nm showed lower heights in the range 1−4 nm, possibly due to compression by the AFM tip. As expected from our LSM observations at the air/water interface, no islands were found by AFM at $\pi = 5$ or 15 mN/m, and the density of islands found by AFM at $\pi = 65$ mN/m was considerably higher than that at $\pi = 30$ mN/m. Islands of all sizes reappeared with repeated scans. (A) Representative AFM image of a film transferred at $\pi = 30$ mN/m. (B) Higher magnification, contrast-enhanced scan of the boxed area in (A), with a height profile.

Domain Stability and the Collapse Transition. Despite the static roughness formation and budding in the region surrounding the domains, neither topographic instability occurs within the domains until monolayer collapse via budding at $\pi \geq 71$ mN/m. A qualitative inspection (Figure 2C−G) and a quantitative analysis (Figure 3B) of LSM micrographs shows that the fractional area covered by the dark domains declines negligibly over the pressure range of $13 \leq \pi < 71$ mN/m. Analysis of the increase with pressure of the domain intensity in LSM images shows that the time-averaged topography of the domains remains flat, at least up to $\pi = 67.3$ mN/m.[7] Finally, as the system is compressed across the collapse plateau at $\pi \geq 71$ mN/m, the domains shrink when buds proliferate across the entire interface

(images not shown). The emergence of static roughness within the domains between 67.3 and 71 mN/m would likely lead to immediate budding. This is not observed, and therefore we conclude that the domains remain flat (gain no static roughness)until they collapse via budding at $\pi \geq 71$ mN/m. The observation that L-DPPC monolayers collapse via budding indicates that budding within the roughened region at lower pressures can be viewed as a precursor to the collapse transition.

Monolayer Bending and Thermal Fluctuations. Both static roughness and thermal fluctuations should facilitate the budding process by bending the monolayer. Because only the region of static roughness shows budding prior to collapse, the roughness must lower the activation barrier to reach the bud state. Because only monolayer bending at wavelengths of order 10−100 nm is expected to provide sufficiently high curvature to promote the budding process, we surmise that the static roughness extends down to wavelengths below the range detected by LSM. In contrast, monolayer bending at wavelengths near 1 μm should have little impact on budding. The proliferation of buds in the roughened region at $\pi = 60$ mN/m and in the domains at $\pi \geq 71$ mN/m likely are due to the increasing thermal fluctuation amplitude that diverges when the surface tension approaches 0 mN/m (π approaches 72 mN/m). The rms roughness of L-DPPC monolayers on water at $T = 23$ °C has been measured by X-ray reflectivity to be $\langle\zeta\rangle = 4.4 \pm 0.1$ Å at $\pi = 45.8$ mN/m.[27] From this value we can calculate the rms roughness at higher pressures using the dependence of thermal roughness on the surface tension ($\langle\zeta\rangle \propto \sqrt{1/\gamma}$) determined by the statistical mechanics of fluctuating interfaces.[28] We obtain $\langle\zeta\rangle \sim 6.5$ Å at $\pi = 60$ mN/m and $\langle\zeta\rangle \sim 23$ Å at $\pi = 71$ mN/m. Remarkably, before bud proliferation at $\pi = 71$ mN/m, the domains withstand fluctuations with amplitude roughly equivalent to the monolayer thickness. The considerably lower roughness threshold for bud proliferation in the roughened region illustrates the degree to which the static roughness promotes budding.

Control Experiments. To address the possibility that these topographic instabilities are due to systematic or sample artifacts, experiments were repeated with different samples of high-purity L-DPPC from two suppliers and with lipids other than L-DPPC. The static roughness formation and budding of L-DPPC have been observed in more than 13 independent experiments employing multiple lipid samples from both Avanti and Sigma. We have never failed to observe these phenomena with the present sensitivity of the LSM. All the monolayers of other compounds (L-DMPE, L-DPPG, and PDA) were compressed through a LE → TC transition,[14,29] and all showed better LSM contrast than L-DPPC at the LE/TC edges, but none showed evidence of static roughness upon disappearance of the LE phase. We cannot exclude the possibility that static roughness emerged in one or more of these systems with wavelength(s) outside the range detectable with LSM. Despite the lack of detectable corrugation, L-DPPG monolayers in the TC phase did undergo a budding transition at $\pi \sim 20$ mN/m, similar to that observed for L-DPPC. The budding transition was not observed in PDA. In L-DMPE monolayers compressed at the standard rate used in this study (0.6 Å^2/mol/min), a small number of point scatterers emerged along narrow, curved lines of contact between adjacent TC domains when the LE phase disappeared. At higher compression rates, increasing numbers of point scatterers appeared along these domain contact lines. Evidently, kinetics are an important factor in the budding of L-DMPE (M. Antia, manuscript in preparation). Experiments with L-DPPC monolayers compressed at higher rates show no apparent changes in static roughness formation or budding. Given the reproducible variation in behavior among different lipid monolayers of similar high purity, we conclude that the topographic instabilities of L-DPPC are not due to sample or systematic artifacts.

Conclusions

These newly found nanoscale topographic transitions in L-DPPC monolayers have several implications. The shape similarity between the flat domains above $\pi = 13$ mN/m and the TC domains grown partway across the LE → TC plateau at $\pi \sim 5$ mN/m indicates that the region of the monolayer that converts from LE to TC in the later stages of the plateau becomes unstable to static roughness formation and budding. This suggests that topographic instabilities originate in an accumulation of packing defects on the periphery of TC domains during the LE → TC transition. The formation of packing defects is expected given the conflicting molecular orientation between the chiral TC domains, as discussed above. Furthermore, the connection between defects and layer bending in two-dimensional systems is well-established. Theoretical studies have shown that flexible, crystalline membranes will buckle out of the plane to relieve the strain fields associated with dislocation and disclination defects[30] or grain boundary networks.[31] And lattice faults in the crystalline protein monolayers known as S layers, which serve as the outermost cell envelope for certain bacteria, have been implicated in the formation of curved membrane structures.[32] Therefore, we propose that the LE → TC transition of L-DPPC creates a spatial distribution of packing defects in which defect-poor chiral domains are surrounded by defect-rich regions that possess lower yield strength against static roughness formation and budding.

The exact nature of the defects and their formation remains to be determined in future experiments. While one might expect the monolayer to yield along narrow grain boundaries, the static roughness occurs over rather wide regions surrounding the core of each domain. The formation of isolated buds suggests the presence of point defects in the roughened region. The lack of static roughness formation and budding in control experiments with PDA indicates that conflicting chain tilt orientation between TC domains is not sufficient to cause topographic transitions in all condensed monolayers. Additional factors may be important such as the headgroup orientation, which is coupled to the chain orientation, and the size of the headgroup relative to the chains. Furthermore, the compression-rate dependence of budding in L-DMPE monolayers indicates an important role for kinetics in some monolayers.

Because a film highly enriched in L-DPPC is widely thought to coat the lung,[15,16] our finding of bud proliferation at high surface pressures provides one possible explanation for the multilamellar structures detected by electron microscopy in alveolar surface films.[33] At $T = 22$ °C, the fluctuation-driven acceleration of budding occurs at a threshold pressure of $\pi = 60$ mN/m. Because thermal roughness increases as $\langle\zeta\rangle \propto \sqrt{T/\gamma}$, bud proliferation at $T = 37$ °C should occur at $\pi \approx 52$ mN/m, near the low end of the physiological pressure range $45 \leq \pi \leq 70$ mN/m.

The static roughness and buds also might be present in condensed lipid bilayer systems because they are found in the range of pressure values ($\pi = 30-35$ mN/m) that evidence suggests corresponds to an internal lateral pressure of bilayers.[34] Such surface topography could, for example, impact the force/distance equilibrium between condensed bilayers.[35]

In summary, LSM has revealed that condensed L-DPPC monolayers at the air/water interface are not flat but possess a

complex, nanoscale topography over a wide surface pressure range. The findings indicate that packing defects can be created on the peripheries of TC domains during the LE → TC transition, that the spatial distribution of these defects can be recorded in the fully condensed monolayer, and that the defects can serve as a source of precollapse instabilities upon compression far below the collapse pressure. The ability to visualize these subtle phenomena and quantify scattered intensities[7] suggests the potential of LSM for future discoveries across the spectrum of science at fluid interfaces.

Acknowledgment. We gratefully acknowledge discussions with G. Wegner on the budding process, and we thank W. Frey for insightful contributions to the development of our BAM and LSM microscopes. We thank M. Antia, B. Piknova, B. Discher, and J. Hall for experimental assistance. We thank the University of Washington Center for Nanotechnology for use of the AFM. These studies were supported by NIH Grants HL3502 and HL60914, NASA Grant NAG8-1149, and funds from the Whitaker Foundation and the American Lung Association of Oregon.

References and Notes

(1) "Tilted-condensed (TC)" is used in place of "liquid-condensed (LC)" following the proposed nomenclature change in the review: Kaganer, V. M.; Möhwald, H.; Dutta, P. *Rev. Mod. Phys.* **1999**, *71*, 779.

(2) Adamson, A. W.; Gast, A. P. *Physical Chemistry of Surfaces*, 6th ed.; John Wiley & Sons: New York, 1997; Chapter 4.

(3) Lipp, M. M.; Lee, K. Y. C.; Takamoto, D. Y.; Zasadzinski, J. A.; Waring, A. J. *Phys. Rev. Lett.* **1998**, *81*, 1650.

(4) Saint-Jalmes, A.; Gallet, F. *Eur. Phys. J. B* **1998**, *2*, 489.

(5) Fradin, C.; Braslau, A.; Luzet, D.; Alba, M.; Gourier, C.; Daillant, J.; Grübel, G.; Vignaud, G.; Legrand, J. F.; Lal, J.; Petit, J. M.; Rieutord, F. *Physica B* **1998**, *248*, 310.

(6) Pluta, M. *Advanced Light Microscopy*; Elsevier: New York, 1989; Vol. 2 pp 91−113.

(7) Schief, W. R.; Hall, S. B.; Vogel, V., submitted for publication.

(8) Hénon, S.; Meunier, J. *Rev. Sci. Instrum.* **1991**, *62*, 936.

(9) Hönig, D.; Möbius, D. *J. Phys. Chem.* **1991**, *95*, 4590.

(10) Weis, R. M.; McConnell, H. M. *Nature* **1984**, *310*, 47.

(11) McConlogue, C. W.; Vanderlick, T. K. *Langmuir* **1997**, *13*, 7158.

(12) Moy, V. T.; Keller, D. J.; Gaub, H. E.; McConnell, H. M. *J. Phys. Chem.* **1986**, *90*, 3198.

(13) Weidemann, G.; Vollhardt, D. *Colloids Surf. A* **1995**, *100*, 187.

(14) Weidemann, G.; Vollhardt, D. *Biophys. J.* **1996**, *70*, 2758.

(15) Goerke, J. J.; Clements, J. A. In *Handbook of Physiology−The Respiratory System*; Macklem, P. T., Mead, J., Eds.; American Physiological Society: Washington, DC, 1985; Vol. 3, pp 247−261.

(16) Keough, K. M. W. In *Pulmonary Surfactant: From Molecular Biology to Clinical Practice*; Robertson, B., Van Golde, L. M. G., Batenburg, J. J., Eds.; Elsevier: Amsterdam, 1992; pp 109−164.

(17) Koynova, R.; Caffrey, M. *Biochim. Biophys. Acta* **1998**, *1376*, 91.

(18) The phase transitions of L-DPPC on water as detected by BAM and LSM, including static roughness formation and budding, were similar to those found on buffer, except that on water the arms of the flat domains were thinner and deformed more easily during compression, and the budding above $\pi = 60$ mN/m covered nearly the entire monolayer. The isotherms on water and buffer were indistinguishable.

(19) Irrespective of the angular-integrated scattered intensity, the upper and lower bubble extremities scatter light into cones that are not collected by the LSM objective (Arimoto, R.; Murray, J. M. *Biophys. J.* **1996**, *70*, 2969).

(20) The lack of scattering from edges nearly parallel to the plane of incidence indicates that both the gas bubble and the TC domain edges are smooth in-plane on the micron scale.

(21) Helm, C. A.; Möhwald, H.; Kjaer, K.; Als-Nielsen, J. *Europhys. Lett.* **1987**, *4*, 697.

(22) Goerke, J.; Gonzales, J. *J. Appl Physiol.* **1981**, *51*, 1108.

(23) Compression−expansion cycles up to $\pi = 40$ mN/m showed minimal hysteresis, but in cycles extending above the shoulder at $\pi \sim 55$ mN/m and below collapse at $\pi = 71$ mN/m, the expansion and recompression showed a shift to lower area, indicating loss of material onto the ribbon barrier (not shown). Furthermore, isotherms of L-DPPC monolayers on the leak-proof continuous interface of a captive bubble confirm the trough leakage. Under similar experimental conditions, the captive bubble isotherm from $\pi = 0$ to $\pi = 71$ mN/m is indistinguishable from that in the ribbon trough except there is no shoulder at $\pi = 55$ mN/m and no evidence of material loss (Crane, J. M.; Putz, G.; Hall, S. B. *Biophys. J.* **1999**, *77*, 3134).

(24) Wiese, W.; Harbich, W.; Helfrich, W. *J. Phys.: Condens. Matter* **1992**, *4*, 1647.

(25) Lipowsky, R. *J. Phys. II* **1992**, *2*, 1825.

(26) Bangham, A. D.; Morley, C. J.; Phillips, M. C. *Biochim. Biophys. Acta* **1979**, *573*, 552.

(27) Daillant, J.; Bosio, L.; Harzallah, B.; Benattar, J. J. *J. Phys. II* **1991**, *1*, 149.

(28) Langevin, D.; Meunier, J. In *Micelles, Membranes, Microemulsions, and Monolayers*; Gelbart, W. M., Ben-Shaul, A., Roux, D., Eds.; Springer: New York, 1994; pp 485−515.

(29) Hönig, D.; Overbeck, G. A.; Möbius, D. *Adv. Mater.* **1992**, *4*, 419.

(30) Seung, H. S.; Nelson, D. R. *Phys. Rev. A* **1988**, *38*, 1005.

(31) Carraro, C.; Nelson, D. R. *Phys. Rev. E* **1993**, *48*, 3082.

(32) Pum, D.; Messner, P.; Sleytr, U. B. *J. Bacteriol.* **1991**, *173*, 6865.

(33) Schürch, S.; Green, F. H. Y.; Bachofen, H. *Biochim. Biophys. Acta* **1998,** *1408*, 180.

(34) Marsh, D. *Biochim. Biophys. Acta* **1996**, *1286*, 183.

(35) Gawrisch, K.; Ruston, D.; Zimmerberg, J.; Parsegian, A.; Rand, R. P.; Fuller, N. *Biophys. J.* **1992**, *61*, 1213.

(36) Experiments show that nonlipid particles can originate from the air, water, buffer salts, and possibly organic solvents. These particles are usually undetectable in BAM. Control experiments with lipid monolayers other than L-DPPC which contained nonlipid particles but did not show static roughness formation or budding demonstrate that nonlipid particles do not cause these topographic transitions.

(37) National Institutes of Health. http://rsb.info.nih.gov/nih-image/ (accessed Oct 1998).